# Temperature dependence of the collision-induced light scattering by $CH_4$ gas

F. Barocchi and A. Guasti
*Dipartimento di Fisica, Università di Firenze, Largo Enrico Fermi 2, 50125 Firenze, Italy*

M. Zoppi
*Istituto di Elettronica Quantistica del Consiglio Nazionale delle Ricerche, Via Panciatichi 56/30, 50127 Firenze, Italy*

S. M. El-Sheikh and G. C. Tabisz
*Department of Physics, University of Manitoba, Winnipeg, Manitoba, Canada R3T 2N2*

N. Meinander
*Department of Physics, University of Helsinki, Siltavuorenpenger 20M, 00170 Helsinki, Finland*
(Received 11 October 1988)

The two-body collision-induced light-scattering spectrum of gaseous $CH_4$ was studied as a function of temperature from 295 K to that of the saturated vapor, 130 K. Models to explain both the induced translational and rotational scattering worked well over this wide temperature range. The validity of a fixed-parameter expression for the pair polarizability important to the translational scattering was shown to hold approximately. Values of the dipole-quadrupole and dipole-octopole polarizabilities were consistent with earlier determinations and served to confirm the applicability of the long-range model of the induction mechanism giving the rotational scattering. The contribution of bound dimers to the spectrum was identified and its temperature evolution studied.

## I. INTRODUCTION

Collision-induced light scattering from simple systems has been studied for over two decades. Much progress has been made in the understanding of the scattering mechanism, especially for the gas phase.[1-3] Models have been developed to describe the interactions leading to the scattered intensity, but these have been tested almost exclusively in the liquid or in the gas phases at 295 K. A detailed study of the scattering by gases as a function of temperature has, in fact, never been done. This paper reports the measurement and analysis of the pair spectrum of gaseous $CH_4$ from 295 to 130 K.

$CH_4$ is an ideal molecule for such an investigation as its spectrum contains features which highlight several aspects of induced scattering. The spectrum consists essentially of an intense, pure translational component and a weaker induced rotational wing. Effects due to scattering by bound dimers[4-6] and to the quantum nature of the collision dynamics[7] are expected to become increasingly important to the translational component with decreasing temperature. Induced rotational Raman scattering was first identified in the $CH_4$ spectrum.[8] It is a particularly propitious example in that the rotational wing clearly extends beyond the translational component over a broad frequency range. The two contributions may then be studied independently, in contrast to a situation such as for $SF_6$, where there is considerable overlap of the two components.[9]

The leading term in the pair polarizability which gives rise to the translational scattering by spherical molecules is due to the first-order dipole-induced dipole (DID) interaction. Small intermediate- and short-range overlap contributions also play a role.[10] This pair polarizability has recently been modeled with an expression containing a single adjustable parameter.[11] Moreover, this parameter has been shown to scale approximately with the dipole polarizability $\alpha_0$ and the molecular separation at the potential minimum $r_m$; specifically, the scaling factor is $6\alpha_0^2/r_m^3$. The model was developed from spectra at 295 K and its temperature dependence has never been investigated. The spectrum of bound dimers appears as a low-frequency feature on the translational component and has been studied in $CH_4$,[4] Ar,[5] and Xe.[6] Prengel and Gornall[4] have given a detailed discussion of the $CH_4$ dimer spectrum at 300 K and 115 K; the dimer spectra of rare gases have been studied only at low temperature. The quantum aspect of the molecular dynamics of a particle as light as $CH_4$ has been treated by Wigner-Kirkwood quantum corrections to the spectral moments.[7] Induced rotational scattering has been interpreted by means of pair-polarizability terms which arise from a long-range interaction mechanism involving high-order multipole polarizabilities, such as the dipole-quadrupole (tensor A) and dipole-octopole (tensor E) polarizabilities.[8] For all intensity and profile calculations, the intermolecular potential plays an important role and the best available form must be chosen.

This paper assesses the validity of these models and the concomitant choice of parameter values in the description of the experimental spectra.

## II. EXPERIMENTAL DETAILS

The experiments reported here were performed at the Istituto di Elettronica Quantistica, Consiglio Nazionale

 

delle Ricerche (IEQ, CNR), Firenze, and the apparatus used is described in detail elsewhere.[12] The gas sample was contained in a pressure cell[13] housed in an Air Products cryogenic cooling system. Gas pressures were measured to a few parts in 1000. Temperatures were recorded to ±0.1 K with calibrated platinum-resistance sensors affixed to the exterior of the cell. Excitation of the spectra was achieved with an argon-ion laser operating at 1 W at 5145 Å. The spectra were obtained with a Spex scanning double monochromator fitted with a Varian VPM-1645 photomultiplier cooled to −40 °C, where the background noise level was 0.07 counts/s. To calibrate intensities in absolute terms, low-pressure $H_2$ was used as an external intensity standard and the light scattered at 20 $cm^{-1}$ from $CH_4$ was compared to the intensities of the $S_0(0)$ and $S_0(1)$ lines of $H_2$. Because the spectrum of $CH_4$ extends 500 $cm^{-1}$ from the exciting line, it was important to correct for variation in the intensity response of the spectrometer-detector system over this range. The response was measured with a calibrated tungsten filament lamp. Experiments were performed in the depolarized geometry, i.e., both the *HV*- and *HH*-polarization components[12] of the scattered light were recorded.

A common procedure[1,14] is to record spectra at a number of densities and then to apply a virial expansion of the intensity at a large number of frequencies to separate two-, three-, and four-body correlation components of the total spectrum. Such an approach was impracticable in the present case. The necessity of recording precise data for an extremely broad spectrum, frequently under low-signal conditions, required long observation times. This circumstance, coupled with stability problems with the cryostat system at low temperature, prevented collection of data for a thorough density analysis. Consequently, another approach was adapted; gas pressures were chosen so that experiment was always performed in a thermodynamic state, for which the intensity varied essentially as the density squared and, thereby, the two-body correlation spectrum was measured directly. Our previous work on $CH_4$ at room temperature was used as a guide for this procedure.[14,15] For example, at 295 K the spectra were recorded from 4 to 15 $cm^{-1}$ with a gas pressure of 10 bars. At higher frequencies the intensity is much weaker and higher gas pressures were required to obtain an adequate signal. Accordingly, the pressures were increased to 40 bars for the region 10–150 $cm^{-1}$ and 90 bars for 100–550 $cm^{-1}$. In these frequency and pressure ranges, the intensity varies quadratically, as demonstrated in accordance with the earlier detailed analysis of Ref. 14. The same approach was applied to spectra recorded at lower temperatures, 250, 200, and 160 K. The spec-

TABLE I. Intensity $D_{\|}$ at 20 $cm^{-1}$ frequency shift.

| $T$ (K) | $D_{\|}$ ($10^{-53}$ $cm^6$) |
|---|---|
| 295.0 | 5.4±0.3 |
| 250.5 | 5.6±0.2 |
| 203.0 | 5.8±0.5 |
| 163.4 | 5.9±0.3 |
| 130.8 | 5.85±0.3 |

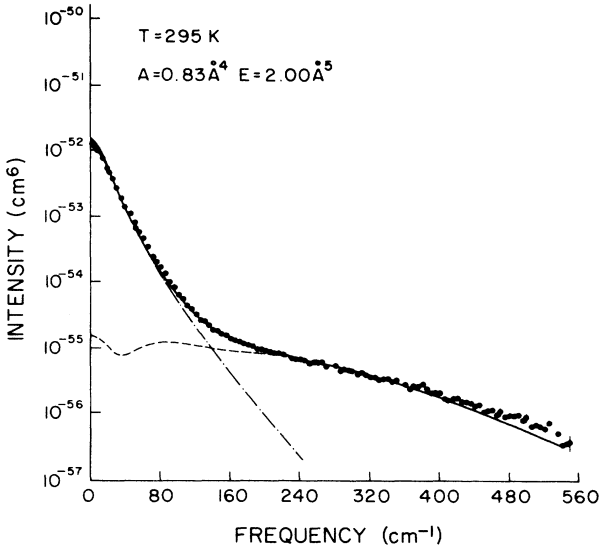


FIG. 1. Induced scattering spectrum of $CH_4$ at 295.0 K. Experimental spectrum (dots); calculated pure translational spectrum including the dimer contribution (dotted-dashed line); calculated rotational spectrum (dashed line); total calculated spectrum (solid line). The values of $A$ and $E$ indicated are those found to give the best fit to the intensity of the rotational wing. Error bars are indicated on the experimental points at high frequency; at low frequency the error is smaller than the size of the point.

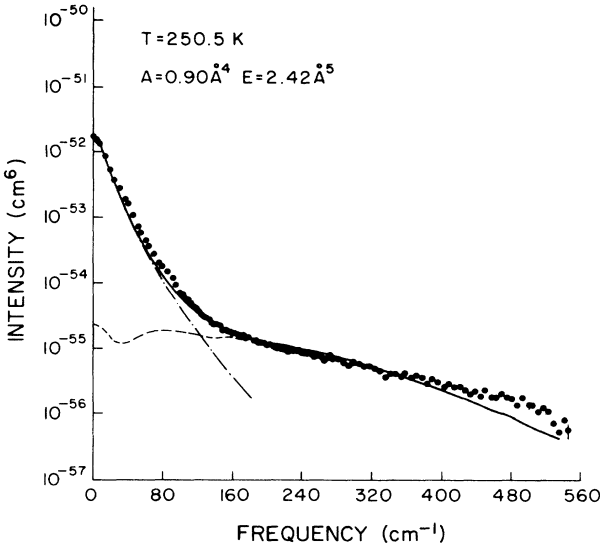


FIG. 2. Induced scattering spectrum of $CH_4$ at 250.5 K. Experimental spectrum (dots); calculated pure translational spectrum including the dimer contribution (dotted-dashed line); calculated rotational spectrum (dashed line); total calculated spectrum (solid line). The values of $A$ and $E$ indicated are those found to give the best fit to the intensity of the rotational wing. Error bars are indicated on the experimental points at high frequency; at low frequency the error is smaller than the size of the point.

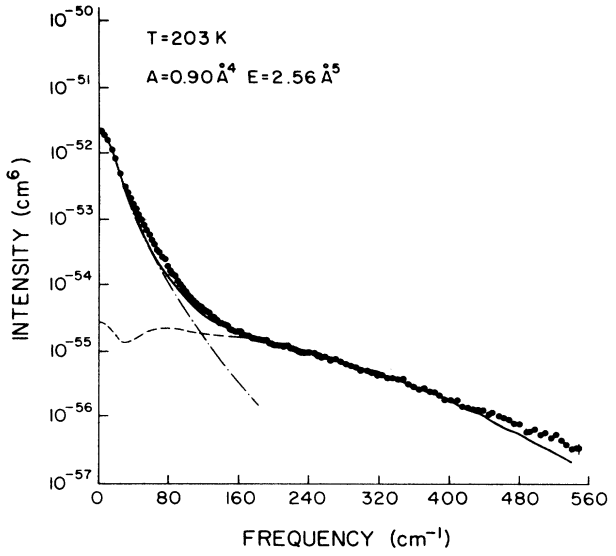


FIG. 3. Induced scattering spectrum of $CH_4$ at 203.0 K. Experimental spectrum (dots); calculated pure translational spectrum including the dimer contribution (dotted-dashed line); calculated rotational spectrum (dashed line); total calculated spectrum (solid line). The values of $A$ and $E$ indicated are those found to give the best fit to the intensity of the rotational wing. Error bars are indicated on the experimental points at high frequency; at low frequency the error is smaller than the size of the point.

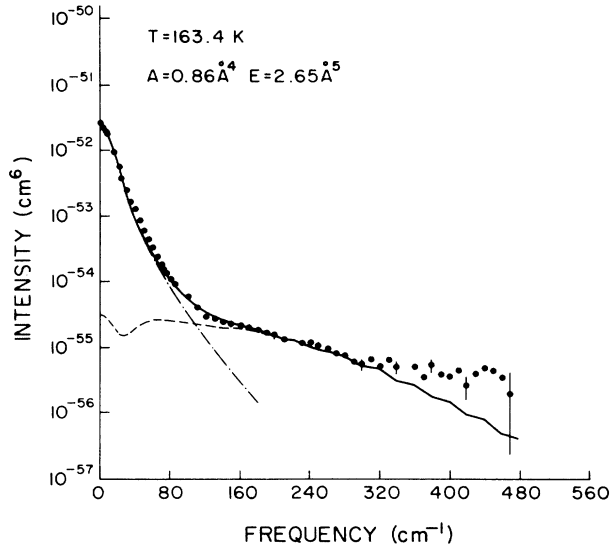


FIG. 4. Induced scattering spectrum of $CH_4$ at 163.4 K. Experimental spectrum (dots); calculated pure translational spectrum including the dimer contribution (dotted-dashed line); calculated rotational spectrum (dashed line); total calculated spectrum (solid line). The values of $A$ and $E$ indicated are those found to give the best fit to the intensity of the rotational wing. Error bars are indicated on the experimental points at high frequency; at low frequency the error is smaller than the size of the point. The structure in the total calculated spectrum at high frequency is due to the narrowing of the individual rotational lines with decreasing temperature.

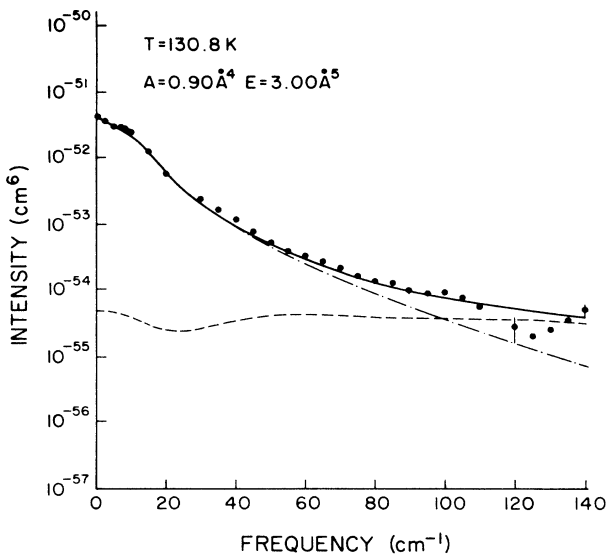


FIG. 5. Induced scattering spectrum of $CH_4$ at 130.8 K. Experimental spectrum (dots); calculated pure translational spectrum including the dimer contribution (dotted-dashed line); calculated rotational spectrum (dashed line); total calculated spectrum (solid line). The values of $A$ and $E$ indicated are those found to give the best fit to the intensity of the rotational wing. Error bars are indicated on the experimental points at high frequency; at low frequency the error is smaller than the size of the point.

trum at 130 K was that of the saturated vapor pressure, 3.48 bars. At these temperatures a detailed density analysis was not available, but confidence in the procedure was gained from the fact that the two- and three-body spectra were known to behave similarly; for example, the zeroth spectral moments of both spectra increase with decreasing temperature.[14–16] Also, the three-body spectrum contributes only at low frequencies,[14] 0–40 $cm^{-1}$. An intensity measurement was always made at 20 $cm^{-1}$ at two different pressures to verify quadratic behavior. Spectra were recorded at different pressures in overlapping frequency regions to ensure continuity in intensity calibration as well as to check quadratic density dependence.

The spectral slit widths were 0.6 $cm^{-1}$ (4–10 $cm^{-1}$), 1.0 $cm^{-1}$ (4–20 $cm^{-1}$), and 2.4 $cm^{-1}$ (10–600 $cm^{-1}$). Densities were computed from $PVT$ data given in Ref. 17. The reduced temperature $T^*$ of the experiments varies from 0.70 to 1.64; $T^*=kT/\varepsilon$, where $\varepsilon$ is the depth of the intermolecular potential.

The final spectra from 6 $cm^{-1}$ are shown in Figs. 1–5. The intensity is presented as $D_{\|}(\nu)=(V)(\partial^2\sigma/\partial\Omega\,\partial\nu)$, where $V$ is the scattering volume, $\sigma$ is the scattering cross section, $\Omega$ is a solid angle, and $\nu$ is the frequency in $cm^{-1}$. The intensities at 20 $cm^{-1}$ given explicitly in Table I should prove useful for future comparison with theory.

## III. CALCULATION OF SPECTRUM

Theoretical spectra were generated under the assumption of no translational-rotational coupling. The transla-

tional and rotational components of the spectra could then be treated independently.

### A. Translational scattering

The translational profile was calculated by a method based on an empirical pair-polarizability anisotropy[11] $\beta(r)$ derived from the first four even classical moments of the depolarized pure translational spectra of the inert gases and methane. This expression is given as

$$\beta(r)=6\alpha_0^2 r^{-3}+\mathcal{A}r^{-6}-\mathcal{B}\exp(-r/r_0)\ . \tag{1}$$

Here, $r$ is the intermolecular distance and $\alpha_0$ is the dipole polarizability of the free molecule. The terms in $r^{-3}$ and $r^{-6}$ are the first- and second-order DID contributions. The coefficient $\mathcal{A}$ is taken in its dispersion-corrected form,[18]

$$\mathcal{A}=6\alpha_0^3+\gamma C_6/3\alpha_0\ , \tag{2}$$

where $\gamma$ is the second hyperpolarizability and $C_6$ is the first dispersion-force coefficient. The third term accounts for short-range overlap effects; $r_0$ is a range parameter scaled from *ab initio* calculations on the He-He interaction.[19] The amplitude $\mathcal{B}$ has been determined from the measured spectral moments at 295 K and has been found to scale as $\mathcal{B}^*=\mathcal{B}(r_m^3/6\alpha_0^2)$. The values of the parameters for $CH_4$ are $\alpha_0=2.642$ Å$^3$, $\gamma=19.2\times10^{-62}$ C$^4$ m$^4$ J$^{-3}$, $C_6=129.6$ a.u., $B^*=2580$, and $x_0=r_0/r_m=0.095\,31$.[11]

The classical symmetric profile, corrected for detailed balance,[20] was then determined for the Stokes side through a computer calculation of the dynamics of the encounter of two $CH_4$ molecules. Details on this procedure have been presented previously.[2,21,22]

The computation is based on the formulas

$$D_{\parallel}(\nu)=\tfrac{6}{45}k_0k_s^3c\int_0^\infty dv\,P(v)\int_0^\infty db\,2\pi bv\Gamma(\nu)\ ,$$

$$\Gamma(\nu)=1.5\left[\int_0^\infty\beta(t)\cos[2\phi(t)+2\pi c\nu t]dt\right]^2+\left[\int_0^\infty\beta(t)\cos(2\pi c\nu t)dt\right]^2+1.5\left[\int_0^\infty\beta(t)\cos[2\phi(t)-2\pi c\nu t]dt\right]^2\ .$$

Here, $k_0$ and $k_s$ are the wave vectors of the incident and scattered radiation, $P(v)$ is the Maxwell distribution of the relative velocities of the colliding pairs, $b$ is the impact parameter, and $\phi$ is the angle swept by the radius vector $\mathbf{r}$ connecting the pair.

To implement the procedure, an intermolecular potential must be employed that controls the dynamics of the encounter. The one chosen was the modified anisotropic Righini-Maki-Klein (RMK) potential[23] described by Meinander and Tabisz.[24] An effective isotropic potential which produces the angular average of the pair distribution function $g(r)$ was constructed at each experimental temperature,[25]

$$g(r)=\exp[-U_{\rm eff}(r)/kT]=\frac{1}{(4\pi)^2}\int\int\exp[-U(r,\Omega_1,\Omega_2)/kT]d\Omega_1 d\Omega_2\ .$$

This effective potential was written in the Hartree-Fock-dispersion (HFD) form:

$$U_{\rm eff}(x)=\varepsilon[Cx^y\exp(-ax)-f(x)(C_6x^{-6}+C_8x^{-8}+C_{10}x^{-10})]\ ,$$

$$f(x)=\begin{cases}\exp\{-[(D/x)-1]^2\}, & x\le D\\ 1, & x>D\ ,\end{cases}$$

$$x=r/r_m\ .$$

As the temperature decreases, the well depth increases and the distance of the potential minimum $r_m$ and the molecular diameter $\sigma$ decrease. All of the potential parameters are listed in Table II, and the potentials are shown for 295 and 130.8 K in Fig. 6. The effective potential or effective pair distribution function is an established technique used to incorporate the effect of the anisotropic part of the potential into a calculation.[25] This is a general procedure and there has been no modification of the potential to suit the present application.

The profiles calculated in this manner arise from the effects of free-free transitions, but do not account for transitions involving bound dimers. These are, however, included in the closed, analytical sum-rule expressions[22] for the classical moments of $D_{\parallel}(\nu)$, $M_{2n}=\frac{2}{15}k_0^4M'_{2n}$, where

TABLE II. Effective potential parameters.

| Parameters \ $T$ (K) | 295.0 | 250.0 | 203.0 | 163.4 | 130.8 |
|---|---|---|---|---|---|
| $C$ | $0.106\,941\times10^8$ | $0.894\,842\times10^7$ | $0.842\,970\,2\times10^7$ | $0.747\,645\,9\times10^7$ | $0.622\,694\,4\times10^7$ |
| $y$ | 2.671 64 | 2.528 48 | 2.513 727 | 2.442 912 | 2.312 344 |
| $a$ | 16.144 07 | 15.960 06 | 15.892 86 | 15.764 64 | 15.5703 |
| $C_6$ | 1.016 033 | 1.018 077 | 1.020 732 | 1.023 577 | 1.026 516 |
| $C_8$ | 0.686 782 5 | 0.689 667 3 | 0.693 426 9 | 0.697 673 | 0.702 353 2 |
| $C_{10}$ | 0.470 044 7 | 0.473 049 8 | 0.476 977 5 | 0.481 494 9 | 0.486 579 5 |
| $D$ | 1.248 246 | 1.250 609 | 1.252 382 | 1.254 463 | 1.256 861 |
| $\epsilon$ (K) | 180.43 | 181.2526 | 182.3238 | 183.6378 | 185.222 |
| $r_m$ (Å) | 4.1465 | 4.141 981 | 4.136 119 | 4.129 256 | 4.121 379 |
| $\sigma$ (Å) | 3.6915 | 3.687 125 | 3.680 639 | 3.673 404 | 3.665 473 |

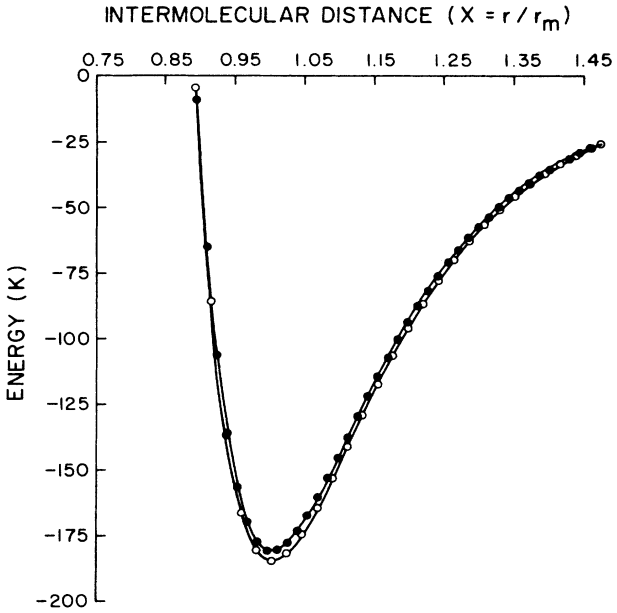


FIG. 6. Effective potential of $CH_4$-$CH_4$ in the region of the minimum: 295.0 K (solid circles); 130.8 K (open circles).

$$M_0' = 4\pi \int_0^\infty \beta^2(r) g(r) r^2 \, dr \ , \tag{3}$$

$$M_2' = 4\pi \frac{kT}{\mu} \int_0^\infty \left[ \left( \frac{d\beta}{dr} \right)^2 + \frac{6\beta^2}{r^2} \right] g(r) r^2 \, dr \ . \tag{4}$$

The expressions[7,26] for $M_4'$ and $M_6'$ are more complicated, but still simply involve $\beta(r)$ and $U(r)$ and their derivatives. The expressions for the moments can be corrected for quantum-mechanical effects on the dynamics by Wigner-Kirkwood terms.[7] To include dimer and quantum-mechanical contributions to the profile, moments $M_0$–$M_6$ were calculated with Eq. (1) and the effective potential. $M_0$, $M_2$, and $M_4$ were corrected for quantum-mechanical effects up to $\hbar^2$; unfortunately, expressions for these corrections to $M_6$ are unavailable. These results were compared with the moments obtained from the intensity $D_\parallel(\nu)$ of the computed profile,

$$M_{2n} = \int_0^\infty (2\pi c \nu)^{2n} D_\parallel(\nu) d\nu \ , \tag{5}$$

which were significantly smaller (Table III). The differences between the two sets of moments were then used to model approximately the dimer band profile as the sum of a Gaussian and an exponential.[27] Even though this choice is one of line-shape engineering, this model has been applied successfully to the significant dimer contribution in the induced scattering spectrum of $SF_6$ at 295 K.[9] This dimer band was then added to the profile due to free-free transitions. In this manner, the translational profile is computed with no adjustable parameters, although below 30 $cm^{-1}$ it is affected by the assumption that the profile is a Gaussian plus an exponential.

### B. Induced rotational scattering

Tetrahedral molecules have an isotropic molecular dipole polarizability $\alpha_0$ and therefore do not exhibit allowed pure rotational Raman scattering. They do, however, possess nonzero anisotropic dipole-quadrupole (A) and dipole-octopole (E) polarizabilities. The interaction of a pair of such molecules with the electric field of an incident light beam gives a pair polarizability modulated by

TABLE III. Calculated spectral moments where the first row in each temperature group is calculated from the computed profile [Eq. (5)], the second row in each temperature group is calculated with the analytical sum rules [Eqs. (3), (4), etc.], and the third row in each temperature group is the value of the second row in each temperature group plus second-order quantum corrections. Percentages show change from the first row.

| $T$ (K) | $M_0'$ ($10^{-70}$ $cm^9$) | $M_2'$ ($10^{-69}$ $cm^9 ps^{-2}$) | $M_4'$ ($10^{-67}$ $cm^9 ps^{-4}$) | $M_6'$ ($10^{-64}$ $cm^9 ps^{-6}$) |
|---|---|---|---|---|
| 295.0 | 1.81 | 3.87 | 6.71 | 4.24 |
| | 2.14 (18%) | 4.00 (3%) | 6.76 (1%) | 4.25 (0.1%) |
| | 2.13 (18%) | 4.02 (4%) | 7.10 (6%) | |
| 250.5 | 1.82 | 3.44 | 5.40 | 3.15 |
| | 2.26 (25%) | 3.63 (6%) | 5.50 (2%) | 3.15 (0%) |
| | 2.26 (25%) | 3.65 (6%) | 5.88 (9%) | |
| 203.0 | 1.83 | 3.00 | 4.18 | 2.21 |
| | 2.50 (36%) | 3.30 (10%) | 4.35 (4%) | 2.22 (1%) |
| | 2.48 (35%) | 3.33 (11%) | 4.82 (16%) | |
| 163.4 | 1.85 | 2.65 | 3.33 | 1.61 |
| | 2.86 (55%) | 3.11 (17%) | 3.60 (8%) | 1.65 (3%) |
| | 2.84 (54%) | 3.14 (19%) | 4.18 (26%) | |
| 130.8 | 1.86 | 2.36 | 2.73 | 1.23 |
| | 3.46 (86%) | 3.08 (31%) | 3.16 (16%) | 1.31 (7%) |
| | 3.42 (84%) | 3.13 (33%) | 3.95 (44%) | |

the rotational motion of the molecules and an associated rotational Raman spectrum.

The part of the mean-square polarizability for a pair of identical molecules 1 and 2 that yields the rotational scattering is[8]

$$\langle \alpha_{xz}^2 \rangle = \tfrac{96}{35}\alpha_0^2 A^2 \overline{r^{-8}} + \tfrac{62\,912}{4725} A^4 \overline{r^{-10}} + \tfrac{22}{9}\alpha_0^2 E^2 \overline{r^{-10}} + \cdots , \quad (6)$$

where $x,z$ are space-fixed axes and $A$ and $E$ are the magnitudes of the tensors A and E. The quantity $\overline{r^{-n}}$ is an average over the pair distribution function. The term in $(\alpha_0 A)^2$ gives rise to spectra following the selection rules on the molecular angular momentum $\Delta J = 0, \pm 1, \pm 2, \pm 3$ in one molecule and $\Delta J = 0$ in the other. The term in $(\alpha_0 E)^2$ gives $\Delta J = 0, \pm 1, \pm 2, \pm 3, \pm 4$ and $\Delta J = 0$. The term in $A^4$ gives rise to double transitions, i.e., $\Delta J = 0, \pm 1, \pm 2, \pm 3$ in each molecule of the pair.

Details on the construction of the rotational spectra are given in Refs. 8 and 25. Each rotational $\delta$ function is broadened[25,28] with a translational broadening function associated with an interaction characterized by a tensor of rank $l$ and varying as $r^{-(l+1)}$. The experimentally estimated exponential decay function for the pure translational spectrum at 295 K has a decay constant of 15.5 $cm^{-1}$. It was taken to be characteristic of the DID $r^{-3}$ interaction. Then through the calculations of Posch,[28] the corresponding decay constants for the single $A$ ($r^{-4}$) and double $A$ and single $E$ transitions ($r^{-5}$) were found. Thus the lines due to A and E at 295 K were broadened with Gaussians of half-width at half maximum (HWHM) of 20 and 25 $cm^{-1}$, respectively; these widths were assumed to vary as $\sqrt{T}$. The profile of the total rotational band is not sensitive to the details of the shape of the broadening function, but instead reflects the distribution of the individual rotational lines, as governed by the selection rules, and their relative intensities. A dip in the calculated rotational spectrum in the region of 20 $cm^{-1}$ arises because of the gap between the $\Delta J = 0$ branch and the maxima of the $\Delta J \neq 0$ branches.

There are two "unknowns" in this calculation: the magnitudes $A$ and $E$. The rotational spectrum was added to the pure translational one, and the values of $A$ and $E$ were adjusted to produce agreement with the experimental intensity in the range 200–300 $cm^{-1}$, where the pure translational component has negligible effect.

## IV. COMPARISON OF CALCULATION AND EXPERIMENT

In Figs. 1–5 the experimental profiles are compared with calculation. Overall, the agreement is very good and the principal behavior of the experimental data is reproduced—namely the narrowing of the translational component (0–100 $cm^{-1}$) and the collapsing of the high-frequency rotational wing, both with decreasing temperature. The low-frequency translational profile is well reproduced at all temperatures, except from 0–30 $cm^{-1}$ at 295 and 250 K. At high frequencies, where the induced rotational component dominates, the experimental intensity is well reproduced over very broad frequency ranges to 560 $cm^{-1}$ at 295 K, 400 $cm^{-1}$ for 250 and 200 K, 300 $cm^{-1}$ for 160 K, and 100 $cm^{-1}$ for 130 K. The value of using the effective potential appropriate to each temperature may be seen by comparing Figs. 5 and 7. When the profile is calculated for 130 K using the isotropic potential derived for 295 K, the agreement between calculation and experiment is clearly worse. Now, we shall consider various aspects of the profile in some detail.

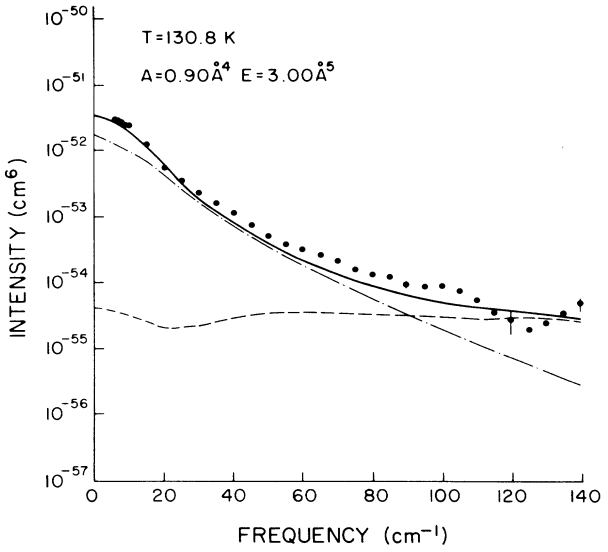


FIG. 7. Induced scattering spectrum at 130.5 K. the calculations were performed with an effective potential appropriate to 295.0 K. Symbols have the same meaning as in Fig. 5.

### A. Dimer spectrum

The low-frequency spectrum has a large contribution from dimers. This can be appreciated from calculation of the classical values of the moments of the translational spectrum (Table III). The full (or "corrected") classical moments calculated from the sum rules (3), (4), etc., and those calculated from the computed profile (only free-free transitions) by Eq. (5) differ by an increasing amount with decreasing temperature. This is particularly true for $M_0'$ and $M_2'$. At 295 K the sum rule $M_0'$ is 18% greater than that for the free pairs; this difference is 86% at 130 K. Similarly, the sum rule $M_2'$ is 3% greater at 295 K and 31% greater at 130 K; the sum rule $M_4'$ is only 1% greater at 295 K and 14% greater at 130 K; the sum rule $M_6'$ is 0.1% greater at 295 K and 7% greater at 130 K. That the differences between the sum-rule values and the moments of the computed profiles are indeed largely due to the dimer contribution was independently confirmed by calculation of the contributions to the moments by bound dimers and free pairs separately with the use of the method described by Levine.[29,30] Quantum-mechanical Wigner-Kirkwood terms produce further changes of 1% or less for $M_0'$ and $M_2'$. However, these effects vary from 5% to 20% for $M_4'$ and could be larger for $M_6'$. In the spectral region where quantum-mechanical corrections to $M_0'$ to $M_4'$ are important, the total calculated profile is approximately correct to order $\hbar^2$; however, this is not true for regions where corrections to $M_6'$ are important.

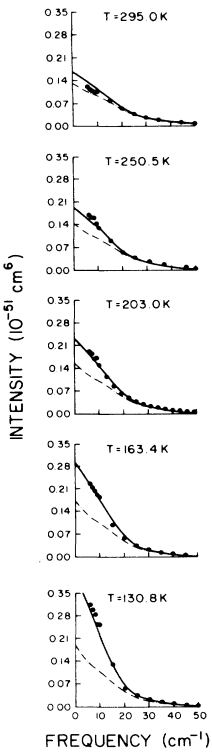


FIG. 8. Intensity of the scattering in the region of the dimer feature at several temperatures. Experimental spectrum (dots)—calculated translational spectrum due to free-free transitions (dotted-dashed line); total calculated spectrum (solid line). Note that the intensity scale is linear, not logarithmic as in Figs. 1–5.

The difference between the free-free profile and experimental data shows dramatically the importance of the dimer spectrum. In Fig. 8 the observed profiles are compared with computed profiles at low frequency on a linear intensity scale. The observed profile is clearly more intense than the profile due to free pairs. The dimer profile calculated from the sum of a Gaussian and an exponential cannot reproduce the dip near zero frequency in the true dimer profile.[4–6] (This dip results from the sum of the various broadened vibrational-rotational branches that constitute the dimer spectrum.) However, the profile used here does adequately represent the evolution of the feature as a function of temperature beyond 6 cm$^{-1}$. The effect of the dimers is negligible in these calculations beyond 30 cm$^{-1}$ at all temperatures. As temperature decreases, the intensity of the dimer peak clearly increases.

### B. Rotational spectrum

There are two adjustable parameters, $A$ and $E$, which determine the magnitude of the induced rotational spectrum. The $\Delta J=0,\pm1,\pm2,\pm3$ branches arising from A dominate those due to the interaction involving E, but at the highest frequencies the $\Delta J=4$ branch of the E spectrum becomes important. Therefore $A$ and $E$ may be determined independently. The values of $A$ found average to 0.88 Å$^4$ and all fall within the range of 0.88±0.05 Å$^5$ reported earlier.[25] This agrees with the *ab initio* calculations of Amos.[25,31] The value of $E$ whose average is 2.5 Å$^5$ also agrees with the earlier estimates.[32] It is evident from the figures that some intensity remains beyond the E spectrum and possibly the multipole series should be taken to higher terms. As a result, the value of $E$ found here must be regarded as an upper limit.

### C. Mid-frequency spectrum

The least satisfactory agreement between theory and experiment occurs at mid-frequencies where the calculated profile lies below experiment from 40 to 160 cm$^{-1}$ for temperatures less than 295 K. Several reasons may be advanced to explain this circumstance. First, it is in this region where quantum-mechanical corrections to higher moments are important. Second, the discrepancy may reflect the use of slightly inappropriate values of $\mathcal{A}$ and $\mathcal{B}$ in (1) at these temperatures, indicating that the scaling law for the polarizability is not exact. Third, the use of an effective isotropic potential instead of the true anisotropic potential can slightly affect the dynamics of the collision and, consequently, the line shape. A full quantum-mechanical line-shape calculation could, in principle, settle these questions. To date, however, no quantum-mechanical calculation with an anisotropic potential has been attempted for induced spectra.

## V. CONCLUSIONS

We now summarize our conclusions.

(1) Models for both the induced pure translational and rotational scattering work well over a range from room temperature to that of the saturated vapor.

(2) It was essential to use an effective potential appropriate to each temperature to reproduce the profile well. For example, at 130 K the discrepancy between theory and experiment is as much as 40% if the effective potential is not employed. The RMK potential was originally developed from solid-state data, the second virial coefficient of the gas, and the known long-range dispersion forces. These results provide an important further test of the RMK potential for $CH_4$ over a range of reduced temperature from 0.7 to 1.6.

(3) The values of the three parameters in the pair polarizability giving the translational scattering have not been adjusted in calculations. As a result, the validity of the scaling of the parameter $\mathcal{B}$ has been shown to hold approximately over this wide temperature range.

(4) The fact that the values of $A=0.88$ Å$^4$ and $E=2.5$ Å$^5$ result in a reproduction of the induced rotational spectrum at all temperatures unequivocably confirms the applicability of the long-range model of the induction mechanism.

(5) Although a rough model was employed to represent the bound-state profile, the agreement with experiment with no adjustable parameters is impressive up to a dimer population which changes the zero moment by 86%.

## ACKNOWLEDGMENTS

We acknowledge fruitful discussions on line shapes with L. Frommhold and M. S. Brown.

[1]G. C. Tabisz, in *A Specialist Periodical Report, Molecular Spectroscopy* (The Chemical Society, London, 1979), Vol. 6, p. 136.
[2]L. Frommhold, Adv. Chem. Phys. **46**, 1 (1981).
[3]*Phenomena Induced by Intermoelcular Interactions,* edited by G. Birnbaum (Plenum, New York, 1985).
[4]A. T. Prengel and W. S. Gornall, Phys. Rev. A **13**, 253 (1976).
[5]D. H. Godfried and I. F. Silvera, Phys. Rev. Lett. **48**, 1337 (1982); Phys. Rev. A **27**, 3008 (1982); **27**, 3019 (1982).
[6]Y. LeDuff, R. Ouillon, V. Chandrasekharan, and B. Silvi, Mol. Phys. **62**, 1065 (1987).
[7]F. Barocchi, M. Moraldi, M. Zoppi, and J. D. Poll, Mol. Phys. **43**, 1193 (1981).
[8]A. D. Buckingham and G. C. Tabisz, Opt. Lett. **1**, 220 (1977); Mol. Phys. **36**, 583 (1978).
[9]S. M. El Sheikh, N. Meinander, and G. C. Tabisz, Chem. Phys. Lett. **118**, 151 (1985).
[10]F. Barocchi and M. Zoppi, in *Phenomena Induced by Intermolecular Interactions,* edited by G. Birnbaum (Plenum, New York, 1985), p. 311.
[11]N. Meinander, G. C. Tabisz, and M. Zoppi, J. Chem. Phys. **84**, 3005 (1985).
[12]U. Bafile, L. Ulivi, M. Zoppi, and F. Barocchi, Phys. Rev. A **37**, 4133 (1988).
[13]P. Mazzinghi and M. Zoppi, Rev. Sci. Instrum. **54**, 1585 (1983).
[14]F. Barocchi, M. Zoppi, D. P. Shelton, and G. C. Tabisz, Can. J. Phys. **55**, 1962 (1977).
[15]D. P. Shelton, G. C. Tabisz, F. Barocchi, and M. Zoppi, Mol. Phys. **46**, 21 (1982).
[16]F. Barocchi, M. Neri, and M. Zoppi, J. Chem. Phys. **66**, 3308 (1977).
[17]*Gas Encylopedia* (Elsevier, Amsterdam, 1976), p. 279.
[18]A. D. Buckingham, Trans. Faraday Soc. **52**, 1035 (1956).
[19]P. D. Dacre, Mol. Phys. **45**, 17 (1982).
[20]F. Barrochi, M. Moraldi, and M. Zoppi, Mol. Phys. **45**, 1285 (1982).
[21]N. Meinander and G. C. Tabisz, J. Quant. Spectrosc. Radiat. Transfer **35**, 39 (1986).
[22]U. Bafile, R. Magli, F. Barocchi, M. Zoppi, and L. Frommhold, Mol. Phys. **49**, 1149 (1983); F. Barocchi, M. Moraldi, and M. Zoppi, Phys. Rev. A **26**, 2168 (1982).
[23]R. Righini, K. Maki, and M. L. Klein, Chem. Phys. Lett. **80**, 301 (1981).
[24]N. Meinander and G. C. Tabisz, J. Chem. Phys. **79**, 416 (1983).
[25]A. R. Penner, N. Meinander, and G. C. Tabisz, Mol. Phys. **54**, 479 (1985).
[26]F. Barocchi, M. Neri, and M. Zoppi, Chem. Phys. Lett. **59**, 537 (1978).
[27]N. Meinander and G. C. Tabisz, Chem. Phys. Lett. **110**, 338 (1984).
[28]H. A. Posch, Mol. Phys. **46**, 1213 (1982).
[29]H. B. Levine, J. Chem. Phys. **56**, 2455 (1971).
[30]N. Meinander (unpublished).
[31]R. D. Amos, Mol. Phys. **38**, 33 (1979).
[32]D. P. Shelton and G. C. Tabisz, Mol. Phys. **40**, 299 (1980).